

# Enhancement of the vortex ratchet effect in superconductor open nanotubes and nanopetals

Rodrigo H. de Bragança<sup>1,2</sup>, Igor Bogush<sup>2,3,4,5</sup>, Oleksandr V. Dobrovolskiy<sup>4,5</sup>, Vladimir M. Fomin<sup>2,3</sup>

<sup>1</sup>*Departamento de Física, Centro de Ciências Exatas e da Natureza,  
Universidade Federal de Pernambuco, Recife, PE, 50740-560, Brasil*

<sup>2</sup>*Institute for Emerging Electronic Technologies, Leibniz IFW Dresden, Helmholtzstraße 20, D-01069 Dresden, Germany*

<sup>3</sup>*Moldova State University, strada A. Mateevici 60, MD-2009 Chisinau, Republic of Moldova*

<sup>4</sup>*Cryogenic Quantum Electronics, Institute for Electrical Measurement Science and Fundamental Electrical Engineering,  
Technische Universität Braunschweig, Hans-Sommer-Str. 66, 38106 Braunschweig, Germany and*

<sup>5</sup>*Laboratory for Emerging Nanometrology, Technische Universität Braunschweig, Langer Kamp 6A-B, 38106 Braunschweig, Germany*

Advancements in the fabrication of superconducting 3D nanostructures, along with the creation of artificial pinning sites, pave the way to novel applications and enhancement of nanosensors, bolometers, and quantum interferometers. The dynamics of magnetic flux quanta (Abrikosov vortices) in 3D nanoarchitectures reveal a rich palette of phenomena unseen in planar counterparts. Here, we consider two types of superconductor 3D nanostructures – open nanotubes and nanopetals – carrying an azimuthal transport current in a homogeneous external magnetic field. The complex 3D geometry of the structures induces an inhomogeneity of the magnetic field and makes the vortices to move along preferred paths. By introducing a lattice of asymmetric pinning sites along these paths, we realize a non-reciprocal flux transport and study a vortex ratchet effect, which is revealed to be stronger than in the respective planar (unrolled) membranes. The enhancement of the vortex ratchet effect becomes apparent via a factor-of-two difference in the depinning current under the current reversal, and it is attributed to the inhomogeneous-field-induced vortex channeling through the areas containing the asymmetric pinning sites. Our results demonstrate that the ratchet efficiency can be enhanced via extending a superconducting film into the third dimension, without increase in the number of asymmetric pinning sites.

## I. INTRODUCTION

Superconductor 3D nanoarchitectures are a subject of vigorous theoretical and experimental studies [1–8] because of fascinating superconducting properties and prospects for applications in nano- and optoelectronics, quantum optics and information processing. In this regard, of special interest are effects emerging because of the extension of planar thin films into the third dimension and the impact of the 3D geometry on phenomena studied extensively for planar strips.

The majority of applications-relevant superconductors are known to be type II superconductors. At moderately strong magnetic fields, these superconductors are penetrated by an array of magnetic flux lines (Abrikosov vortices or fluxons). In some applications, such as, in Abrikosov-vortex random access memory (AV-RAM) [9], vortices play a role of information bits, while in other applications, the presence of (moving) vortices gives rise to undesired dissipation [10, 11].

In order to prevent vortices from generating undesired voltage upon their motion, pinning sites are usually introduced [12] to confine a vortex within a small region of the superconductor, of the order of the coherence length  $\xi$ . Then, in the presence of a transport current, a vortex experiences a driving Lorentz-type force  $F_L$  counterbalanced by a pinning force  $F_p$  created by the pinning sites. Besides, a vortex experiences a vortex-vortex repulsion and interacts with the energy barriers associated with the sample edges [13]. The length scale of this interaction is given by the magnetic field penetration depth  $\lambda$ .

The interaction of a vortex with a pinning site is described using a pinning potential, whereby an asymmetry in the pinning potential gives rise to a *vortex ratchet effect* (VRE) [14]. Usually, vortex ratchets are based on a periodic pinning potential lacking inversion symmetry, and thus, exerting different pinning forces on vortices that move in opposite directions,

giving rise to a rectified voltage under the current reversal and asymmetric current–voltage characteristics (CVC) [14–17]. Previously, various configurations of the pinning potentials were used for studying VREs both theoretically and experimentally. These include random [18] and ordered [19, 20] distributions of pinning sites with an averaged density in the form of a sawtooth wave, stacked arrowheads distributions [21], arrays of in-plane magnetized dipoles [22], arrays of triangular antidots [23] and many others.

Here, we study combined effects of a 3D geometry and an asymmetric pinning potential on the vortex motion in open nanotubes and nanopetals, see Fig. 1. These structures consist of parts of a cylinder with large and small central angle of the arc, correspondingly, and the vortex dynamics therein are compared with those in a flat strip. Previously, it was shown that a maximum of the normal magnetic field component  $B_n$  at a convexity may act as a conveyor for vortices in the context of vortex guiding [7]. In the present study, we focus on the non-reciprocity of magnetic flux transport caused by the presence of the asymmetric pinning sites, since in some ranges of  $B$  and transport currents, the vortices move in one direction easier than in the opposite direction, giving rise to a VRE.

The numerical simulations are performed relying upon the time-dependent Ginzburg-Landau (TDGL) equation, which allows us to obtain the CVCs for the nanoarchitectures under consideration and to calculate the VRE efficiency by comparing the depinning currents under the current reversal. We show that the cooperative action of the inhomogeneous  $B_n$  with the asymmetric pinning potential enhances the VRE for the nanotube and the nanopetal. We attribute this fact to the 3D geometry-induced forcing of vortices to move in the areas with the asymmetric pinning sites, rather than in between those areas, as revealed for the reference planar structure, despite it has a much larger number of pinning sites.

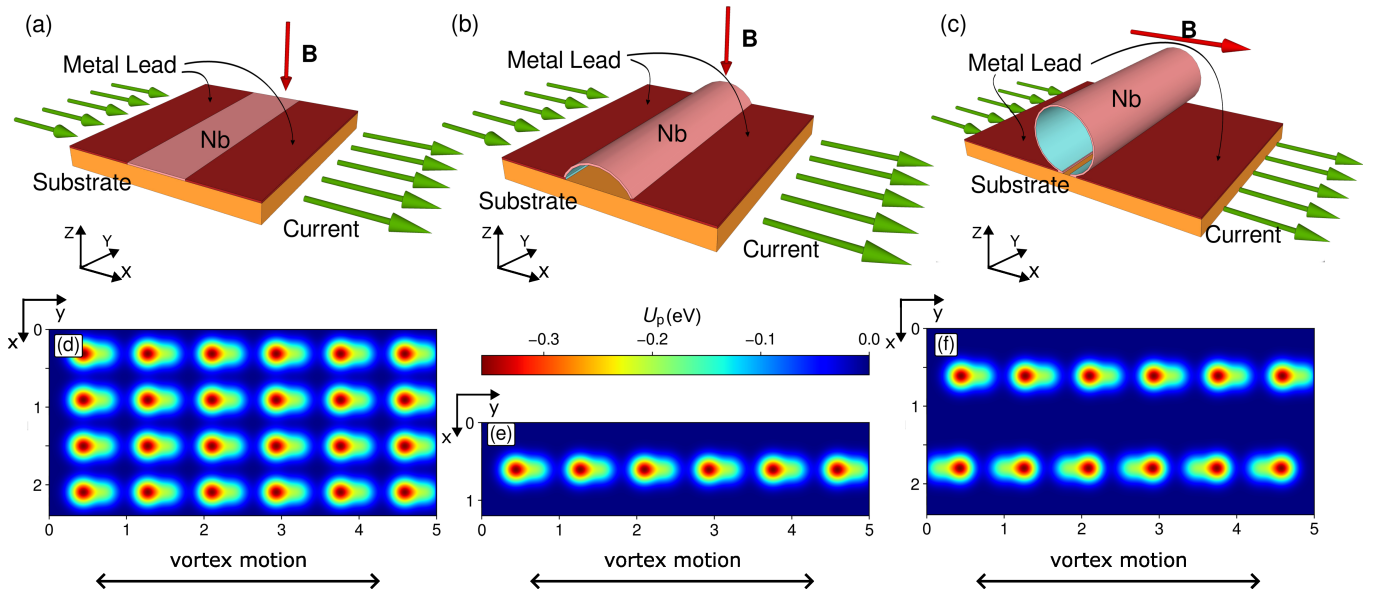


FIG. 1. Geometries (a-c) and configurations of the pinning sites (d-f) for a planar strip (a, d), a nanopetal (b, e), and an open nanotube (c, f).

TABLE I. Material and geometric parameters of the Nb 3D nanoarchitectures used in the TDGL simulations.

Parameters	Denotation	Value for Nb
Electron mean free path	$l$	6 nm
Fermi velocity	$v_F = \sqrt{2E_F/m_e}$	$6 \times 10^{-5}$ m/s
Diffusion coefficient	$D = lv_F/3$	$1.2 \times 10^{-3}$ m <sup>2</sup> /s
Normal conductivity	$\sigma = l/[3.72 \times 10^{-6} \Omega\text{m}^2]$	$16 (\mu\Omega\text{m})^{-1}$
Relative Temperature	$T/T_c$	0.950/0.952/0.955
Penetration depth	$\lambda = \lambda_0 \sqrt{\xi_0/(2.66l/(1-T/T_c))}$	273/278/287 nm
Coherence length	$\xi = 0.855 \sqrt{\xi_0 l/(1-T/T_c)}$	58/60/62 nm
GL parameter	$\kappa = \lambda/\xi$	4.7

## II. MODEL

### A. Geometries under consideration

The dynamics of vortices are studied for the three geometries shown in Fig. 1, in which a superconductor layer is shaped as a flat strip (a), a nanopetal (b), and an open nanotube (c). The structures are placed in a homogeneous magnetic field directed as shown in Fig. 1(a-c) and producing a flux density  $\mathbf{B}$ . A transport current of density  $j_{tr}$  is applied to the structures via a pair of normally conducting leads attached to the slit banks (strip edges), resulting in an azimuthal current flow for the open nanotube and the nanopetal.

The cylindrical surfaces in Fig. 1(b,c) are parametrized with the 2D Cartesian coordinates, the arc-length in the azimuthal direction  $x \in [\delta/2, 2\pi R - \delta/2]$ , and the coordinate along the cylinder axis  $y \in [0, L]$ . The flat nanostrip [see Fig. 1(a)] is described similarly, but the spatial profile of  $\mathbf{B}_n$  is in this case homogeneous. All structures are assumed to be made of Nb films of the thickness  $d = 50$  nm, which allows one to neglect finite-thickness effects [24]. Table I summarizes the material parameters and relations between them in the dirty limit [25].

The flat strip is modeled as a rectangular  $2.39 \times 5 \mu\text{m}^2$  (width,  $W \times$  length,  $L$ ), and the open nanotube as a cylinder of radius  $R = 0.39 \mu\text{m}$  and length  $L = 5 \mu\text{m}$ , with a narrow slit of the arc width  $\delta = 0.06 \mu\text{m}$ . The nanopetal is modeled as a part of a cylinder of a larger radius  $R = 0.951 \mu\text{m}$  (which is easier to manufacture) and the length  $L = 5 \mu\text{m}$ , with a larger slit of arc width  $\delta = 4.78 \mu\text{m}$ . The resulting width for the open nanotube is the same as for the flat strip  $W = 2.39 \mu\text{m}$  and twice smaller than for the nanopetal.

In the open nanotube, there are two groups of vortices moving in opposite directions, see Fig. 1(c) [26]. This is caused by the sign reversal of  $\mathbf{B}_n$  as one maps the tube surface onto a plane. From the previous studies, it is also known that the vortices tend to move in the regions with the maximal  $B_n$  [7, 26]. By contrast, the nanopetals harbour only one group of vortices, all moving in one direction, but, similarly to the open nanotubes, provide vortices with the preferable paths near the region with the maximal  $B_n$ . In what follows, we demonstrate that nanopetals can provide similar vortex ratchet efficiency as nanotubes do, with an advantage of an easier experimental realization. Finally, in the planar structure, all vortices move in the same direction and, due the homogeneity of  $\mathbf{B}_n$ , the vortices move in the entire superconducting strip.

## B. Equations and parameters

The spatiotemporal evolution of the superconducting order parameter  $\psi$  in the nanostructures is described by the time-dependent Ginzburg-Landau (TDGL) equation

$$(\partial_t + i\phi)\psi = (\nabla - i\mathbf{A})^2\psi + (1 - |\psi|^2 + U_p)\psi, \quad (2.1)$$

where  $\phi$  is the scalar potential,  $U_p$  the pinning potential [27], and  $\mathbf{A}$  the vector potential tangent to the surface, which describes the normal component  $B_n = \mathbf{B} \cdot \mathbf{n}$  with  $\mathbf{n}$  being the outer unit vector normal to the (cylindric) surface. In Eq. (2.1), the differential operator  $\nabla$  acts in the tangent space of the surface rather than in the 3D space. Equation (2.1) is written in a dimensionless form for the units reported in Table II. A finite-difference method with a grid resolution of  $12.5 \times 12.5$  nm and a time step of 0.025 ps [28, 29] is used for the solution of the TDGL equation.

The scalar potential satisfies the Poisson equation

$$\nabla^2\phi = \frac{1}{\sigma}\nabla \cdot \mathbf{j}_{\text{sc}}, \quad \mathbf{j}_{\text{sc}} = \mathfrak{I}m(\psi^*(\nabla - i\mathbf{A})\psi), \quad (2.2)$$

where  $\mathbf{j}_{\text{sc}}$  is the superconducting current density. The experimentally observable is the voltage between the normally conducting leads, which is determined by the difference of the scalar potentials at the both leads averaged over their length.

TABLE II. Dimensional units for quantities in Eqs. (2.1) and (2.2).

Parameter	Unit	Value for Nb at $T/T_c = 0.952$
Time	$\xi^2/D$	2.8 ps
Length	$\xi$	60 nm
Magnetic field	$\Phi_0/2\pi\xi^2$	92 mT
Current density	$\hbar c^2/8\pi\lambda^2\xi e$	60 GA m <sup>-2</sup>
Electric potential	$\sqrt{2}H_c\xi\lambda/c\tau$	111 $\mu$ V
Conductivity	$c^2/4\pi\kappa^2D$	31 ( $\mu\Omega$ m) <sup>-1</sup>

## C. Pinning sites

We consider an array of asymmetric pinning sites with the pinning potential  $U_p$  described by the Lorentzian function

$$U_p(x, y; x_p, y_p) = -\frac{U_0}{1 + \left(\frac{x-x_p}{\xi}\right)^2 + \left(\frac{y-y_p}{\xi}\right)^2}, \quad (2.3)$$

where  $(x_p, y_p)$  are the coordinates of the pinning site center and  $U_0$  is the pinning potential depth. The total pinning potential is given by a superposition of two pinning potential troughs, one shallow and one deep [30, 31], see Fig. 2, that results in an asymmetric pinning potential

$$U_p = U_1 + U_2, \quad (2.4)$$

$$U_1(x, y) = U(x, y; x_p, y_p), \quad (2.5)$$

$$U_2(x, y) = \frac{1}{2}U(x, y; x_p, y_p + \Delta p). \quad (2.6)$$

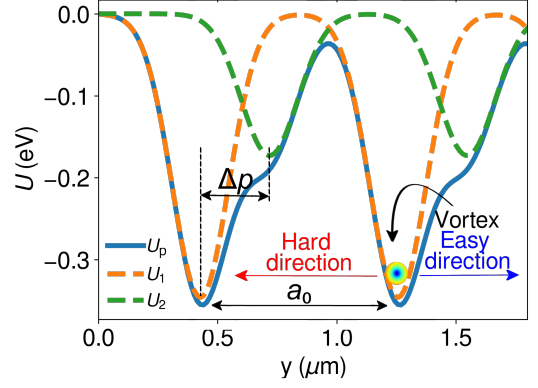


FIG. 2. Pinning potential versus coordinate  $y$  for constant  $x$  as a superposition of one deep and one shallow potential troughs.

The potential trough  $U_2$  is twice shallower than  $U_1$ , and it is shifted by  $\Delta p$  with respect to the coordinate  $y$ , along which the vortices move. The 1D array of pinning potential troughs thus formed is positioned in the middle of the nanopetal [Fig. 1(e)] and in the middle of each half-cylinder in the open nanotube (Fig. 1f), while four arrays of the potential troughs are considered for the flat strip, see Fig. 1(d).

The modeling is done for  $U_0 = 0.348$  eV and  $\Delta p = 0.35a_0$ , where  $a_0 \approx 0.83$  is the period of the pinning potential, and hence, there are six potential troughs along a  $5 \mu\text{m}$ -long nanostructure. This choice of  $a_0$  ensures that there is only one local minimum of  $U_p$  in each pinning potential trough in Fig. 2. If the distance  $\Delta p$  was too large or too small, the difference between the hard and easy directions would be negligible [30]. The pinning force acting on a vortex is determined by the gradient of the pinning potential  $\mathbf{F}_p = -\nabla U_p$ . For the vortex motion from left to right (easy direction) in Fig. 2, a vortex experiences a weaker pinning than for its motion from right to left (hard direction) in the pinning potential.

The average voltage generated by vortices in the nanostructure is calculated as a function of the transport current density  $j_{\text{tr}}$ . As long as  $j_{\text{tr}}$  is smaller than the depinning current density  $j_{\text{dp}}$ , all vortices are pinned. As soon as  $j_{\text{tr}}$  exceeds  $j_{\text{dp}}$ , vortices start moving across the nanostructure, generating a voltage. Due to the VRE, the values of  $j_{\text{dp}}$  differ upon the current reversal. Namely, for the vortex motion in the hard direction  $j_{\text{dp}}^+ > j_{\text{dp}}^-$  for the vortex motion in the easy direction. In what follows, we compare the absolute values  $j_{\text{dp}}^\pm \geq 0$ .

## III. RESULTS

Figure 3 shows the evolution of the resistance of the nanostructures with increase of the transport current  $j_{\text{tr}}$ . An abrupt increase in the resistance with increasing  $j_{\text{tr}}$  points to the depinning of vortices. A nearly constant resistance is indicative of immobile pinned vortices, because close-to-lead areas provide a finite resistance contribution owing to the proximity effect. The vortex depinning depends not only on the transport current density, magnetic field and pinning strength, but on the

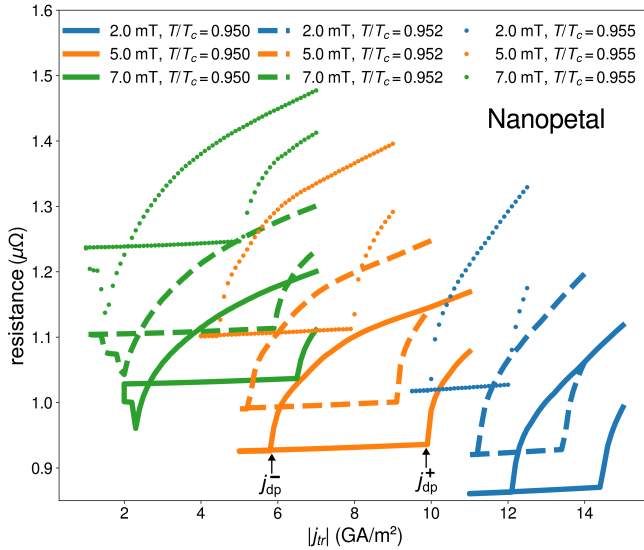


FIG. 3. CVCs for both current directions for the nanopetal. A larger depinning current corresponds to the vortex motion in the hard direction in the asymmetric pinning potential.

presence or absence of nearby vortices as well. Therefore, the vortex depinning is a probabilistic event, and not all vortices in the nanostructure depin at the same value of  $j_{tr}$ . In our analysis, the quantities  $j_{dp}^{\pm}$  denote the values of the transport current density at which at least one vortex is depinned. When all vortices are depinned, the resistance exhibits a linear increase, which points to a regime of free flux flow. Summarizing, three regions in the current dependence of the resistance are distinguished: completely pinned vortices, completely mobile vortices, and a transition between these two regimes.

In order to quantify the efficiency of the VRE, we calculate

$$\eta \equiv \frac{j_{dp}^+ - j_{dp}^-}{j_{dp}^+ + j_{dp}^-} \quad (3.1)$$

as a function of  $B$  for the nanopetal, the nanotube and the planar structure at  $T/T_c = 0.955$ . The results are presented in Fig. 4. The depinning non-reciprocity is significant for the nanopetal and the nanotube, while for the planar structure it is weaker or absent for  $B > 10$  mT. For the nanopetal and the nanotube, the largest efficiency of the VRE is revealed at magnetic fields between 5 and 8 mT. The maximal VRE efficiency  $\eta_{dp} \approx 53\%$  is obtained for the nanopetal at 7 mT.

#### IV. DISCUSSION

*Applicability of the model.* Before entering the discussion of the results, we like first to state the applicability of the model. While the nanoarchitectures under consideration are 3D objects, here their numerical modeling is performed relying upon an effectively 2D TDGL model. The applicability of the 2D model is justified, as long as the membranes are thin enough to neglect finite-thickness effects. First, the film

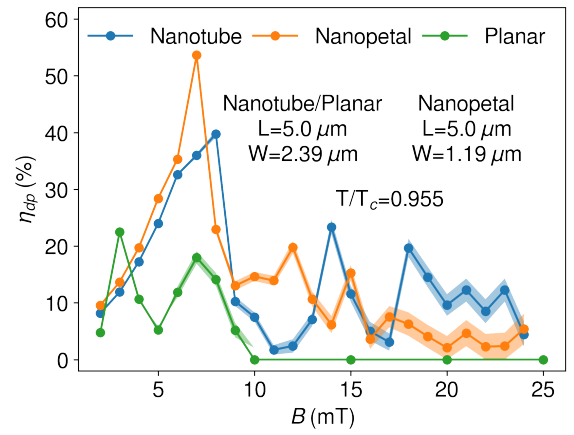


FIG. 4. Vortex ratchet efficiency for the open nanotube, the nanopetal and the flat strip at  $T/T_c=0.955$ . Semi-transparent regions denote the uncertainty in the calculations.

thickness  $d$  must be smaller than the penetration depth,  $d < \lambda$ . This assures negligibility of the induced magnetization affecting the order parameter dynamics. Second, the magnetic field component tangent to the surface can lead to vortex nucleation with cores along the cylinder walls in the paraxial direction, which is suppressed when the thickness is smaller than few  $\xi(T)$ , with  $2\xi(T)$  giving an estimate for the vortex core diameter. Third, large values of the surface curvature lead to the curvature-induced potentials of the da Costa type, which are negligible if the curvature radius  $R$  is much larger than the thickness  $d$  [32–34].

*Enhancement of the ratchet effect in 3D nanostructures.* The key result of our present studies is that the VRE is stronger for the open nanotube and the nanopetal as compared to the planar strip, despite a considerably smaller number of pinning sites in the 3D structures. The spatial distributions of the order parameter in the structures under study, which are shown in Fig. 5, allow for the following explanation of the VRE enhancement. In the nanotube and the nanopetal, the vortices move in the areas, where  $B_n$  is maximal, and the presence of the asymmetric pinning sites along the vortex trajectories enhances the efficiency of the VRE. For the planar strip,  $B_n$  is homogeneous, and there are no preferred areas for the vortex motion, which would be dictated by the magnetic field inhomogeneity. Of course, the vortex trajectories are affected by both, the vortex-vortex and vortex-pinning interactions, but for the planar strip, in order to prevent the vortex motion between the pinning sites, a larger number of pinning sites would be required.

*Vortex trajectories.* An inspection of the vortex trajectories in conjunction with the ratchet efficiency for the planar strip in Fig. 5(a) reveals that the VRE vanishes at  $B > 10$  mT. Indeed, the fundamental vortex matching [15, 35] for the planar strip is expected for  $n = BS/\Phi_0$  vortices ( $S$ : film area). This would yield a fundamental matching field of  $B_m \approx 4.15$  mT in neglect of the edge barriers for the (de)nucleation of vortices and the order parameter suppression along the normally conducting leads. An account for these constraints

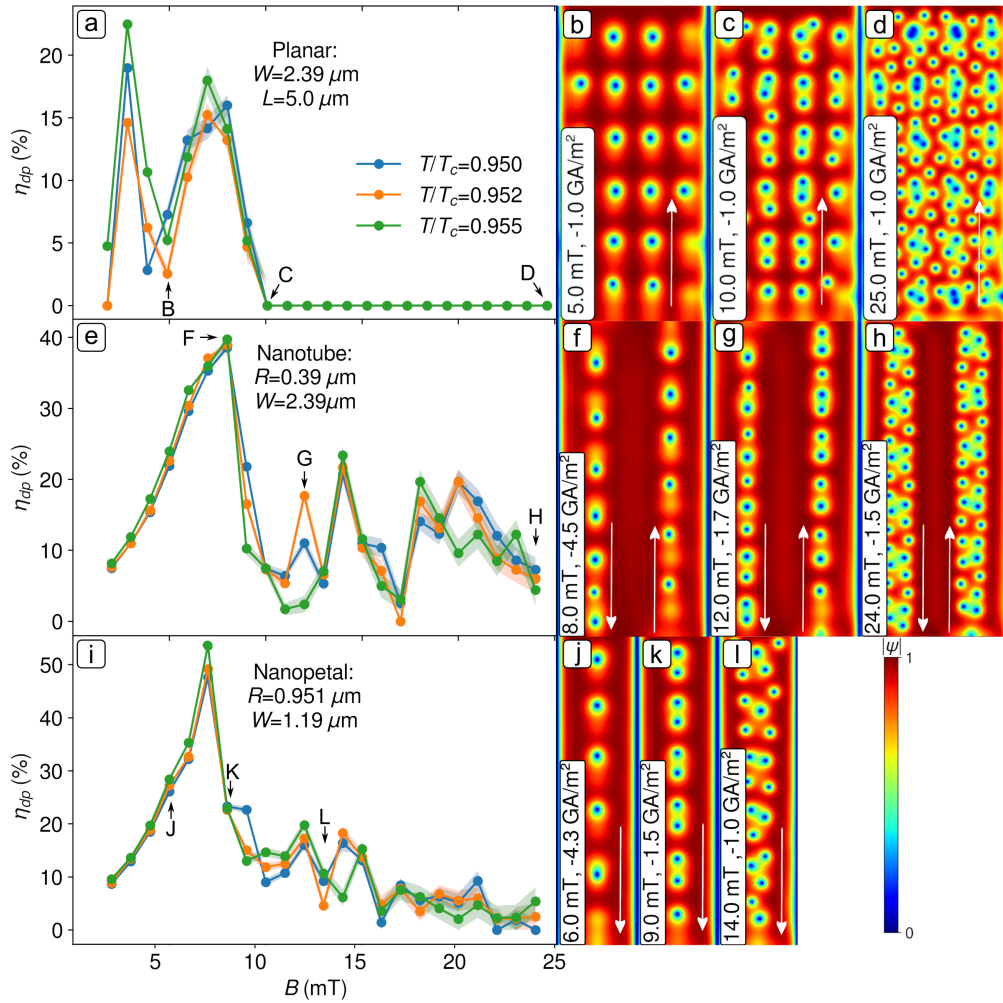


FIG. 5. VRE efficiency (a,e,i) and snapshots of the spatial distribution of the modulus of the superconducting order parameter  $|\psi|$  (b-d,f-h,j-l) in the nanopetal, the nanotube and the planar strip for a series of parameters, as indicated. The arrows in the plots indicate the magnetic field values, for which the configurations of vortices are shown in the contour plots. The semi-transparent regions around the curves denote the uncertainty in the calculations. The white arrows in the color plots indicate the direction of the vortex motion for the positive current polarity.

seems to lead to the fundamental matching configuration at a higher  $B \approx 7 \text{ mT}$ , as suggested by the configurations in Fig. 5(b) and (c), between which the VRE efficiency is maximal. Another maximum in the VRE efficiency at  $3.5 \text{ mT}$  in Fig. 5(a) can be attributed to the configuration, at which the number of pinning sites is equal to the double number of vortices. With an increase of  $B$  above  $10 \text{ mT}$ , the vortex-vortex repulsion stipulates the presence and motion of interstitial vortices between the pinning sites, see Fig. 5(d), thus leading to a vanishing VRE.

For the open nanotube, the dependence of the VRE efficiency on  $B$  in Fig. 5(e) features a series of maxima, while  $\eta$  for the nanotube is larger than  $\eta$  for the planar strip in a broad range of  $B$ . The configurations of vortices in Fig. 5(f-h) suggest that these peaks can be associated with the matching effects for a chain or more complex arrangements of vortices with the periodicity of the pinning site arrays in both half-cylinders. Regardless of the magnetic field value in the stud-

ied range of  $B$ , it is seen that the motion of vortices occurs in the areas, where the asymmetric pinning sites are located, and the location of the pinning site arrays along the positions of the  $B_n$  maxima leads to the vortex guiding along the pinning sites. A similar channeling effect was discussed in our previous work [7] in the context of non-diverging vortex jets in 3D open nanotubes.

Finally, the VRE for the nanopetal exhibits the highest efficiency  $\eta \approx 53\%$  at  $B \approx 7 \text{ mT}$ . As in the open nanotube, the vortices are forced by the inhomogeneous  $B_n$  to move along the pinning site arrays. It is noteworthy, that  $\eta$  for the nanopetal is slightly smaller than for the open nanotube, but this high VRE efficiency is achieved with a twice smaller number of pinning sites (6 pinning troughs in the nanopetal versus 12 in the open nanotube). In this way, the predicted high efficiency of the VRE for the nanopetal makes it to a prospective 3D nanostructure for an experimental examination of the VRE.

*Experimental realization.* The studied geometries can, in principle, be fabricated by established nanofabrication techniques, and hence, the discussed effects appeal for experimental examination. Among the nanofabrication techniques capable of 3D prototyping, two approaches should be mentioned, namely, strain-relaxation-driven self-rolling of thin films [1, 2] and 3D nanoprinting using focused electron- or ion beam-induced deposition (FEBID or FIBID) [3–6, 36–38]. The modelled pinning sites are also realistic and similar to the experimentally studied, e.g., for superconducting Pb [39] and Nb [40] films. While the manufacturing of nanotubes is challenging, the fabrication of nanopetals appears to be easier as one could use, e.g., some scaffold material and deposit a superconducting layer atop, using FEBID/FIBID in conjunction with area-selective deposition [41].

The studied dynamics of vortices in an asymmetric pinning potential imply a weak volume pinning due to the intrinsic disorder or structure of the superconducting membrane. Accordingly, the predicted effects should be examined experimentally for superconductors with a weak background pinning, while the asymmetric pinning sites should be strong pins. For instance, the direct-write superconductor Nb-C satisfies [42] these conditions, and 3D nanostructures made from this material were demonstrated [43]. Further, strong pinning sites can be realized by milling of holes or antidots by a FIB [40] or by decorating the surface of a superconductor with an array of nanomagnets using FEBID/FIBID [5, 44].

## V. CONCLUSION

We have analyzed the vortex ratchet effect in 3D open nanotubes, nanopetals and planar strips with an array of asymmetric pinning sites. Our analysis based on the numerical solution of the TDGL equation has revealed an about factor-of-two enhancement of the vortex ratchet effect in the 3D nanos-

tructures in comparison with the 2D planar strip, despite the factor-of-two larger number of pinning sites in the latter. The enhanced vortex ratchet effect in the studied 3D nanostructures is attributed to the combined effects of the inhomogeneous magnetic field and the asymmetry of the pinning sites. Namely, the motion of vortices occurs in the areas, where the normal component of the magnetic field is maximal, and hence, the vortices are forced to channel along the areas with the strong asymmetric pinning sites.

The suggested approach for an enhancement of the ratchet effect can pave the way towards new developments of superconducting devices, such as on-chip microwave filters and current- and magnetic-field-tuneable high-frequency voltage rectifiers, microwave generators and modulators with low power consumption. As an interesting follow-up study, we anticipate that the efficiency of the vortex ratchet effect can be controlled via deflecting the chain of the moving vortices away from the areas with the pinning sites upon changing the direction of the applied magnetic field [45].

## ACKNOWLEDGEMENTS

R.H.dB. thanks the research funding agency CAPES for the Sandwich Ph.D. scholarship, the IFW for the office space, J. Albino Aguiar for his support and Suívini Bragança for her help with the figures. The authors thank M. D. Croitoru and R. Córdoba for fruitful discussions. Work of I.B. was funded by the Deutsche Forschungsgemeinschaft (DFG, German Research Foundation) under Germany’s Excellence Strategy – EXC-2123 QuantumFrontiers — 390837967. I.B., O.D. and V.M.F. are grateful for the support by the European Cooperation in Science and Technology (E-COST) Action CA21144. Further, O.V.D. acknowledges the E-COST for support via Grant No. E-COST-GRANT-CA21144-5883b676.

- 
- [1] D. J. Thurmer, C. C. Bof Bufon, C. Deneke, and O. G. Schmidt, Nanomembrane-based mesoscopic superconducting hybrid junctions, *Nano Lett.* **10**, 3704 (2010).
- [2] S. Lösch, A. Alfonsov, O. V. Dobrovolskiy, R. Keil, V. Engemaier, S. Baunack, G. Li, O. G. Schmidt, and D. Bürger, Microwave radiation detection with an ultra-thin free-standing superconducting niobium nanohelix, *ACS Nano* **13**, 2948 (2019).
- [3] D. Makarov, O. M. Volkov, A. Kákay, O. V. Pylypovskyi, B. Budinská, and O. V. Dobrovolskiy, New dimension in magnetism and superconductivity: 3D and curvilinear nanoarchitectures, *Adv. Mater.* **34**, 2101758 (2022).
- [4] V. M. Fomin and O. V. Dobrovolskiy, A perspective on superconductivity in curved 3D nanoarchitectures, *Appl. Phys. Lett.* **120**, 090501 (2022).
- [5] R. Córdoba and V. M. Fomin, Topological and chiral superconductor nanoarchitectures, *Appl. Phys. Lett.* **124**, 170501 (2024).
- [6] E. Zhakina, L. Turnbull, W. Xu, M. König, P. Simon, W. Carrillo-Cabrera, A. Fernandez-Pacheco, U. Vool, D. Suess, C. Abert, V. M. Fomin, and C. Donnelly, *Vortex motion in reconfigurable three-dimensional superconducting nanoarchitectures* (2024), [arXiv:2404.12151 \[cond-mat.mes-hall\]](https://arxiv.org/abs/2404.12151).
- [7] I. Bogush, O. V. Dobrovolskiy, and V. M. Fomin, Microwave generation and vortex jets in superconductor nanotubes, *Phys. Rev. B* **109**, 104516 (2024).
- [8] L. Shani, A. N. Michelson, B. Minevich, Y. Fleger, M. Stern, A. Shaulov, Y. Yeshurun, and O. Gang, DNA-assembled superconducting 3D nanoscale architectures, *Nat. Commun.* **11**, 5697 (2020).
- [9] T. Golod, A. Iovan, and V. M. Krasnov, Single abrikosov vortices as quantized information bits, *Nat. Commun.* **6**, 8628 (2015).
- [10] J. Clarke, Chapter 2, SQUIDS: Principles, noise, and applications, in *Superconducting Devices*, edited by S. T. Ruggiero and D. A. Rudman (Academic Press, 1990) pp. 51–99.
- [11] N. Kopnin, *Theory of Nonequilibrium Superconductivity* (Oxford University Press, 2001).
- [12] E. H. Brandt, The flux-line lattice in superconductors, *Rep. Progr. Phys.* **58**, 1465 (1995).
- [13] B. Budinská, B. Aichner, D. Y. Vodolazov, M. Y. Mikhailov, F. Porrati, M. Huth, A. Chumak, W. Lang, and O. Dobrovolskiy,

- Rising speed limits for fluxons via edge-quality improvement in wide MoSi thin films, *Phys. Rev. Appl.* **17**, 034072 (2022).
- [14] A. V. Silhanek, J. Van de Vondel, and V. V. Moshchalkov, Guided vortex motion and vortex ratchets in nanostructured superconductors, in *Nanoscience and Engineering in Superconductivity*, edited by V. Moshchalkov, R. Woerdenweber, and W. Lang (Springer, Berlin, Heidelberg, 2010) pp. 1–24.
- [15] O. Dobrovolskiy, E. Begun, V. Bevez, R. Sachser, and M. Huth, Upper frequency limits for vortex guiding and ratchet effects, *Phys. Rev. Appl.* **13**, 024012 (2020).
- [16] B. L. T. Plourde, Nanostructured superconductors with asymmetric pinning potentials: Vortex ratchets, *IEEE Trans. Appl. Supercond.* **19**, 3698 (2009).
- [17] C. O. Reichhardt and C. Reichhardt, Ratchet effects in active matter systems, *Annu. Rev. Condens. Matter Phys.* **8**, 51 (2017).
- [18] C. J. Olson, C. Reichhardt, B. Jankó, and F. Nori, Collective interaction-driven ratchet for transporting flux quanta, *Phys. Rev. Lett.* **87**, 177002 (2001).
- [19] C. Reichhardt, D. Ray, and C. J. O. Reichhardt, Reversible ratchet effects for vortices in conformal pinning arrays, *Phys. Rev. B* **91**, 184502 (2015).
- [20] C. Olson Reichhardt, Y. Wang, Z. Xiao, W. Kwok, D. Ray, C. Reichhardt, and B. Jankó, Pinning, flux diodes and ratchets for vortices interacting with conformal pinning arrays, *Physica C* **533**, 148 (2017).
- [21] Y. Togawa, K. Harada, T. Akashi, H. Kasai, T. Matsuda, F. Nori, A. Maeda, and A. Tonomura, Direct observation of rectified motion of vortices in a niobium superconductor, *Phys. Rev. Lett.* **95**, 087002 (2005).
- [22] C. C. de Souza Silva, A. V. Silhanek, J. Van de Vondel, W. Gillijns, V. Metlushko, B. Ilic, and V. V. Moshchalkov, Dipole-induced vortex ratchets in superconducting films with arrays of micromagnets, *Phys. Rev. Lett.* **98**, 117005 (2007).
- [23] V. Rouco, A. Palau, C. Monton, N. Del-Valle, C. Navau, A. Sanchez, X. Obradors, and T. Puig, Geometrically controlled ratchet effect with collective vortex motion, *New J. Phys.* **17**, 073022 (2015).
- [24] E. I. Smirnova, R. O. Rezaev, and V. M. Fomin, Simulation of dynamics of the order parameter in superconducting nanostructured materials: Effect of the magnetic field renormalization, *Low Temp. Phys.* **46**, 325 (2020).
- [25] M. Tinkham, *Introduction to superconductivity* (Courier Corporation, 2004).
- [26] V. M. Fomin, R. O. Rezaev, and O. G. Schmidt, Tunable generation of correlated vortices in open superconductor tubes, *Nano Lett.* **12**, 1282 (2012).
- [27] M. P. Sørensen, N. F. Pedersen, and M. Ögren, The dynamics of magnetic vortices in type II superconductors with pinning sites studied by the time dependent ginzburg–landau model, *Physica C* **533**, 40 (2017).
- [28] R. O. Rezaev, E. I. Smirnova, O. G. Schmidt, and V. M. Fomin, Topological transitions in superconductor nanomembranes under a strong transport current, *Commun. Phys.* **3**, 144 (2020).
- [29] I. Bogush and V. M. Fomin, Topological defects in open superconducting nanotubes after gradual and abrupt switching of the transport current and magnetic field, *Phys. Rev. B* **105**, 094511 (2022).
- [30] B. Y. Zhu, L. V. Look, V. V. Moshchalkov, B. R. Zhao, and Z. X. Zhao, Vortex dynamics in regular arrays of asymmetric pinning centers, *Phys. Rev. B* **64**, 012504 (2001).
- [31] V. A. Shklovskij, V. V. Sosedkin, and O. V. Dobrovolskiy, Vortex ratchet reversal in an asymmetric washboard pinning potential subject to combined dc and ac stimuli, *J. Phys. Condens. Matter* **26**, 025703 (2014).
- [32] R. da Costa, Quantum mechanics of a constrained particle, *Phys. Rev. A* **23**, 1982 (1981).
- [33] H. Jensen and H. Koppe, Quantum mechanics with constraints, *Ann. Phys.* **63**, 586 (1971).
- [34] L. Du, Y.-L. Wang, M. Li, J. Gu, L. Zhou, G. Kang, H. Tang, and Q. Chen, Curvature-induced superconductivity enhancement for ultra-thin superconducting films (2023), [arXiv:2205.14373 \[cond-mat.mes-hall\]](https://arxiv.org/abs/2205.14373).
- [35] M. Karrer, B. Aichner, K. Wurster, C. Magén, C. Schmid, R. Hutt, B. Budinská, O. V. Dobrovolskiy, R. Kleiner, W. Lang, E. Goldobin, and D. Koelle, Vortex matching at 6 T in  $\text{YBa}_2\text{Cu}_3\text{O}_{7-\delta}$  thin films by imprinting a 20-nm periodic pinning array with a focused helium-ion beam, *Phys. Rev. Appl.* **22**, 014043 (2024).
- [36] L. Skoric, D. Sanz-Hernández, F. Meng, C. Donnelly, S. Merino-Aceituno, and A. Fernández-Pacheco, Layer-by-layer growth of complex-shaped three-dimensional nanostructures with focused electron beams, *Nano Lett.* **20**, 184 (2020).
- [37] C. Donnelly, A. Hierro-Rodríguez, C. Abert, K. Witte, L. Skoric, D. Sanz-Hernández, S. Finizio, F. Meng, S. McVitie, J. Raabe, D. Suess, R. Cowburn, and A. Fernández-Pacheco, Complex free-space magnetic field textures induced by three-dimensional magnetic nanostructures, *Nat. Nanotech.* **17**, 136 (2022).
- [38] O. M. Volkov, O. V. Pylypovskiy, F. Porrati, F. Kronast, J. A. Fernandez-Roldan, A. Kákay, A. Kuprava, S. Barth, F. N. Rybakov, O. Eriksson, S. Lamb-Camarena, P. Makushko, M.-A. Mawass, S. Shakeel, O. V. Dobrovolskiy, M. Huth, and D. Makarov, Three-dimensional magnetic nanotextures with high-order vorticity in soft magnetic wireframes, *Nat. Commun.* **15**, 2193 (2024).
- [39] L. Embon, Y. Anahory, A. Suhov, D. Halbertal, J. Cuppens, A. Yakovenko, A. Uri, Y. Myasoedov, M. L. Rappaport, M. E. Huber, A. Gurevich, and E. Zeldov, Probing dynamics and pinning of single vortices in superconductors at nanometer scales, *Sci. Rep.* **5**, 7598 (2015).
- [40] O. V. Dobrovolskiy, E. Begun, M. Huth, and V. A. Shklovskij, Electrical transport and pinning properties of Nb thin films patterned with focused ion beam-milled washboard nanostructures, *New J. Phys.* **14**, 113027 (2012).
- [41] F. Porrati, S. Barth, G. C. Gazzadi, S. Frabboni, O. M. Volkov, D. Makarov, and M. Huth, Site-selective chemical vapor deposition on direct-write 3D nanoarchitectures, *ACS Nano* **17**, 4704 (2023).
- [42] O. V. Dobrovolskiy, D. Y. Vodolazov, F. Porrati, R. Sachser, V. M. Bevez, M. Y. Mikhailov, A. V. Chumak, and M. Huth, Ultra-fast vortex motion in a direct-write Nb-C superconductor, *Nat. Commun.* **11**, 3291 (2020).
- [43] F. Porrati, S. Barth, R. Sachser, O. V. Dobrovolskiy, A. Seybert, A. S. Frangakis, and M. Huth, Crystalline niobium carbide superconducting nanowires prepared by focused ion beam direct writing, *ACS Nano* **13**, 6287 (2019).
- [44] O. V. Dobrovolskiy, M. Huth, and V. A. Shklovskij, Anisotropic magnetoresistive response in thin Nb films decorated by an array of Co stripes, *Supercond. Sci. Technol.* **23**, 125014 (2010).
- [45] I. Bogush, V. M. Fomin, and O. V. Dobrovolskiy, Steering of vortices by magnetic field tilting in open superconductor nanotubes, *Nanomaterials* **14**, 420 (2024).